THE JOURNAL OF PHYSICAL CHEMISTRY C

Article

Cite This: J. Phys. Chem. C 2018, 122, 11128−11135

pubs.acs.org/JPCC

Toward a Microscopic Understanding of the Magnetization Behavior of a Multimolecular Single Crystal of Radical-Bridged [Dy^{III}_4] Cubane Units: A Joint Ab Initio, Micro-Superconducting Quantum Interference Device, and Electron Paramagnetic Resonance Study

Veacheslav Vieru,[†] Naoya Iwahara,[†] Dorsa Komijani,[‡] Stephen Hill,[‡] Wolfgang Wernsdorfer,[§,∥,⊥] and Liviu F. Chibotaru*[,†]

[†]Theory of Nanomaterials Group, Katholieke Universitiet Leuven, Celestijnenlaan, 200F, 3001 Leuven, Belgium

[‡]National High Magnetic Field Laboratory and Department of Physics, Florida State University, 1800 E. Paul Dirac Drive, Tallahassee, Florida 32310, United States

[§]Institut Néel, CNRS and Université Grenoble Alpes, BP 166, 25 Avenue des Martyrs, Grenoble 38042, Cedex 9, France

[∥]Institut für Nanotechnologie, Karlsruhe Institute of Technology (KIT), Hermann Von-Helmholtz Platz 1, D-76344 Eggenstein-Leopoldshafen, Germany

[⊥]Physikalisches Institut, Karlsruhe Institute of Technology (KIT), Wolfgang Gaede Street 1, D-76131 Karlsruhe, Germany

Supporting Information

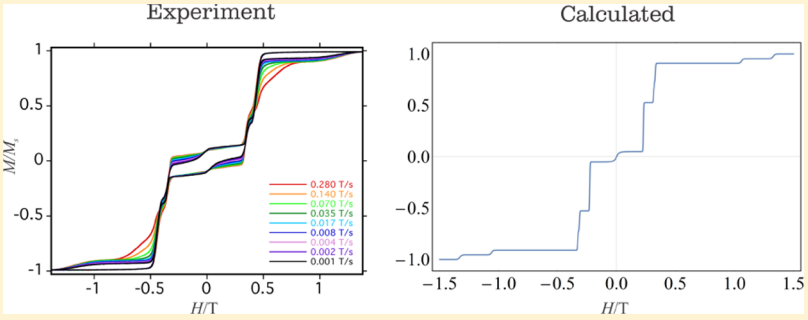

ABSTRACT: The field-dependent magnetization and magnetization blocking in single-crystalline samples of radical-bridged [Dy^{III}_4] cubane units are studied by ab initio calculations, micro-superconducting quantum interference device, and electron paramagnetic resonance. Because of the canted spin structure, a transverse method was applied to detect ferromagnetic and antiferromagnetic projections, for which remarkably different hysteresis magnetization loops were observed and investigated. Given 18 complexes in a unit cell of the crystal, a special ab initio-based approach has been developed to describe the magnetism in this material. The application of this ab initio methodology reveals a remarkable correlation between the evolution of the calculated magnetizations of each of the 18 molecules in the unit cell and the experimentally measured single-crystal hysteresis loop structure. This affords a level of insight into the microscopic magnetic properties that is unprecedented for a spin system of such complexity and highlights the profound influence that crystal-packing effects and molecular orientation can exert on the bulk magnetic properties of molecule-based materials.

1. INTRODUCTION

Single-molecule magnets (SMMs) are molecular compounds which possess an energy barrier to the magnetization reversal.[1,2] As a result, they show slow relaxation of magnetization and magnetic hysteresis loops at low temperatures. This makes them promising candidates for utilization in high-density storage devices, quantum computing, and spintronics.[3−6] One of the main condition for a molecule to perform as a good SMM is the presence of magnetic ions with high anisotropy and large magnetic moments.[7,8] This requirement makes the lanthanide ions ideal candidates for the design of SMMs. Notably, compounds based on Dy^{III}, Tb^{III}, Ho^{III}, and Er^{III} ions have shown remarkably high barriers and large coercive fields in the hysteresis loops.[9−13] For the investigation of SMMs, magnetization hysteresis loop measurements became routinely used and are amongst the most frequently employed techniques. Despite their frequent application, the theoretical analysis of the observed magnetization-field dependence is often lacking. Herein, we present a detailed ab initio study of magnetic properties of a single-crystal with unit cells containing

Received: February 14, 2018
Revised: April 17, 2018
Published: April 22, 2018

DOI: 10.1021/acs.jpcc.8b01582
J. Phys. Chem. C 2018, 122, 11128−11135

18 radical-bridged dysprosium clusters with the formula $[Dy_4(\mu_3\text{-}OH)_4(BpyTz^{\bullet-})_2(OAc)_2(acac)_4]\cdot THF$ (**1**), $BpyTz^{\bullet-}$ = radical anion of 3,6-bis(3,5-dimethylpyrazol-1-yl)-1,2,4,5-tetrazine (Figure 1). The synthesis and description of the crystal structure will be published elsewhere; here, we report the magnetization hysteresis loops and electron paramagnetic resonance (EPR) measurements and their description and ab initio-based interpretation within a dedicated approach. Given the high structural and magnetic complexity of **1**, the microscopic rationalization of its properties is rather unprecedented, keeping promises for successful investigation of other complex magnetic molecular materials.

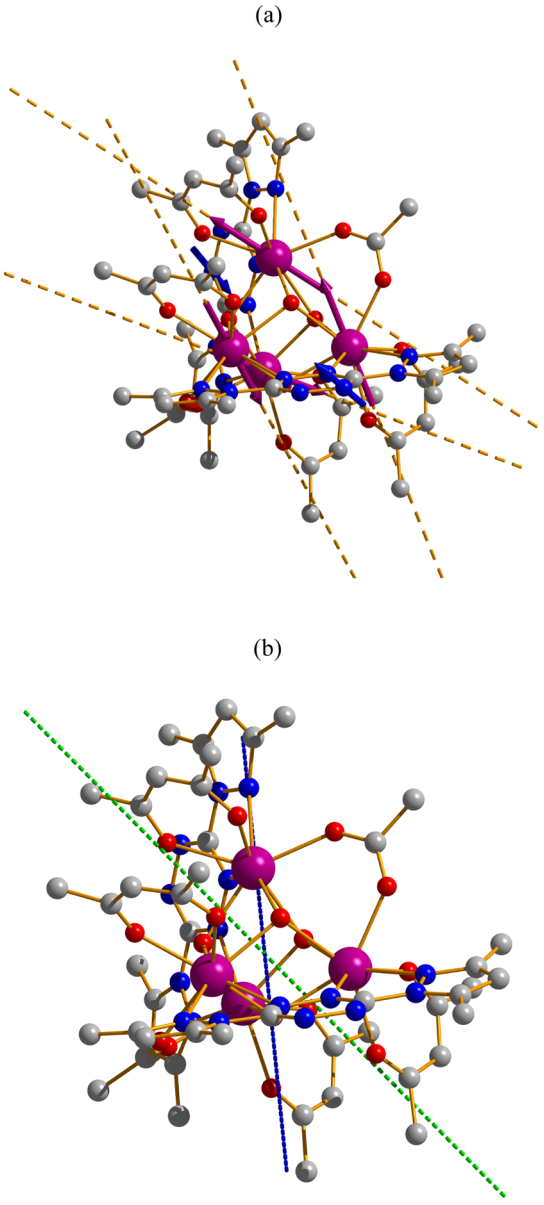

Figure 1. Molecular structure of $[Dy^{III}_4]$ cluster with omitted H atoms. (a) Dashed lines show the orientation of the main magnetic axis in the ground state of Dy^{III} ions, whereas the arrows show the orientation of the corresponding magnetic moments in the ground exchange doublet. (b) Blue dashed line shows the orientation of the main magnetic axis in the ground exchange doublet, whereas the green line shows the orientation of the main magnetic axis in the first excited exchange doublet. Color scheme: Dy = pink, O = red, N = blue, and C = gray.

2. COMPUTATIONAL METHODOLOGY

Broken-symmetry calculations (BS-DFT) on the experimentally determined structure have been carried out employing the B3LYP functional and SVP basis set as implemented in the ORCA 3.03 program.[14] All ab initio calculations were done by using Molcas 8.0 program package.[15] Including all four Dy^{III} ions in the active space is computationally impossible, that is why the calculations were done on individual dysprosium centers. Considering that the complex is too large to be calculated by ab initio methods, we considered Dy fragments as shown in Figure S4 by keeping the experimentally determined positions of atoms and only omitting the atoms located far from the corresponding Dy center. The neighboring Dy^{III} ions were replaced with Lu^{III}. Atomic natural orbitals (ANOs) from the Molcas ANO-RCC library were used for all atoms: ANO-RCC-VTZP for Dy, nearest O and nearest N atoms, and bridging H atoms and ANO-RCC-VDZ for the rest of the atoms. To save disk space, the Cholesky decomposition threshold was set to 1×10^{-8}. The active space of the CASSCF calculation included nine electrons spanned by seven 4f orbitals of Dy^{III} ion. The obtained spin-free states were later mixed by spin−orbit coupling within SO-RASSI program. Because of disk space limitations, only 21 sextet, 128 quartet, and 130 doublet states were included in the calculation. On the basis of the resulted spin−orbital states, SINGLE_ANISO program was used for the computation of local magnetic properties of Dy^{III} ions.[16] Having obtained the local properties of Dy centers, the exchange interactions were considered within the Lines model[17] by using POLY_ANISO program.[18]

3. RESULTS AND DISCUSSION

Hysteresis loop measurements were carried out on single crystals of **1** in the 0.03−5 K temperature regime using a custom-built micro-superconducting quantum interference device (SQUID) apparatus.[19] The spins within **1** appear to be canted with respect to one another, that is, tilted by some angle from their internuclear axis, such that it is not possible to apply the magnetic field along a global easy-axis. Using the transverse-field method,[20] we detected an average antiferromagnetic and ferromagnetic projection among the spins so as to apply the field along these two directions. Thus, two sets of hysteresis loops were collected (Figures 2 and S1). All of these loops in general display steplike features, which are typical for exchange-biased resonant quantum tunneling as a result of antiferromagnetic interactions between the constituent magnetic centers. Complex **1** shows both temperature and sweep rate-dependent hysteresis loops below approximately 1.6 K (Figures 2 and S1), unambiguously confirming SMM behavior. In particular, for the first step around zero field, a large coercive field opens upon cooling. This behavior is typical of an SMM with very slow zero-field relaxation, similar to previous observations made in respect of some Dy^{III}-containing compounds.[21,22] The relaxation time (τ) of **1** was extracted from decay measurements of the dc magnetization over the temperature range of 1.3−0.03 K (Figures S2a and S3a).[23] Because of the wide distribution of multiple relaxation processes, a roughly linear fit performed in the thermal regime to an Arrhenius equation gave the effective energy barrier U_{eff} and preexponential factor τ_0: $U_{eff}/k_B \approx 12.4$ K (8.6 cm^{-1}) and $\tau_0 \approx 1.3 \times 10^{-6}$ s for the ferromagnetic projection (Figure S2b) and $U_{eff}/k_B \approx 9.8$ K (6.8 cm^{-1}) and $\tau_0 \approx 2.7 \times 10^{-5}$ s for the antiferromagnetic projection (Figure S3b). The relaxation time

DOI: 10.1021/acs.jpcc.8b01582
J. Phys. Chem. C 2018, 122, 11128−11135

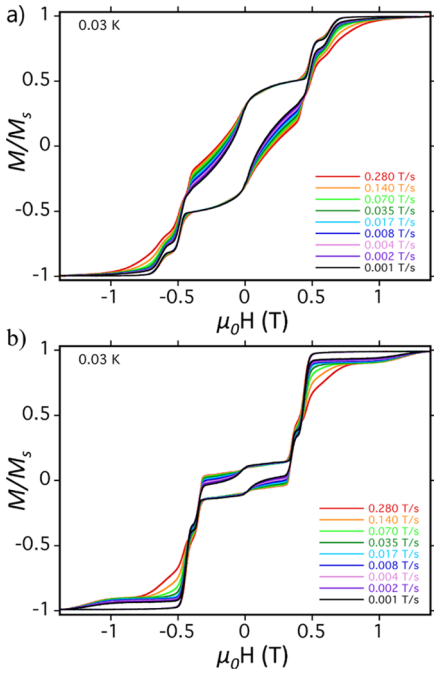

Figure 2. Magnetization (M) vs field (H) hysteresis loops for a single crystal of **1** at 0.03 K at the indicated sweep rates, where in (a) the magnetic field is applied along the average ferromagnetic projection and in (b) the field is applied along the average antiferromagnetic projection (see the text for details). M is normalized to its saturation values M_s, at 1.4 K.

obtained here is relatively slow and at the lower end of the experimental range typically seen in polymetallic Dy^{III} compounds.[24,25]

To prove the presence of radicals in **1**, EPR spectroscopy measurements were carried out on an isostructural compound with Dy^{III} ions replaced by diamagnetic Lu^{III} ones, $[Lu_4(\mu_3\text{-}OH)_4(BpyTz^{\bullet-})_2(OAc)_2(acac)_4]$ (**2**) (see Supporting Information for details). Details of synthesis and X-ray structure of **2** will be reported elsewhere. The observed strong/narrow signal in the EPR spectrum of **2** can clearly be attributed to a bulk response (Figure S9), establishing the presence of unpaired radical spins. A slight shift of the position of these signals with the orientation of the applied field is attributed to a combination of nonisotropic demagnetization in the non-symmetric single-crystal sample and, potentially, to a weak exchange anisotropy between radical spins (see below). Attempts to observe a similar radical EPR signal in **1** were unsuccessful, suggesting appreciable exchange coupling to Dy. To get additional evidence for the presence of two radicals in **2**, the BS-DFT calculations have been done. These calculations indeed show the existence of two well-separated radicals, delocalized in $N_2C_2N_2$ tetrazine rings at the opposite sides of the complex (Figure 3). Interestingly, for each radical, a large domain of opposite magnetization is observed on the corresponding C_2 group, which is due to the spin polarization mechanism similar to the one discussed in ref 26. The BS-DFT calculation also yields the value of the exchange coupling constant, J = 0.29 cm^{-1} (employing Yamaguchi's formula[27]). The small value of the exchange interaction between the radicals is not surprising, given the large distance between them.

To establish a microscopic understanding of the magnetic properties of **1**, the electronic structure of individual Dy ions in

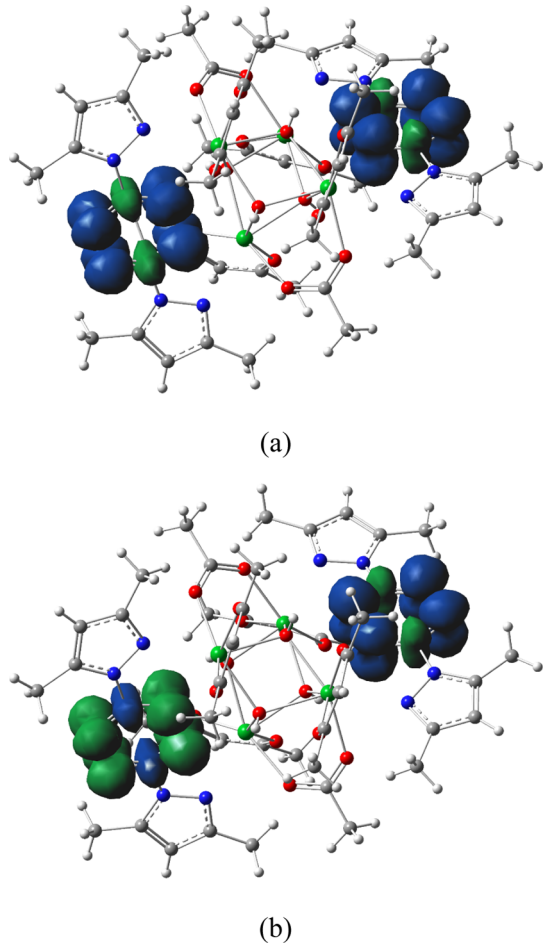

Figure 3. Spin-density plots of high-spin calculation (a) and broken-symmetry calculation (b) in **2** showing the existence of two radicals. The blue color denotes domains with positive spin density, whereas the green color denotes domains with negative one. Isovalue for the spin-density surface was set to 0.002. Color scheme: Lu = green, O = red, N = blue, C = gray, and H = white.

the $[Dy^{III}_4]$ cluster has been investigated. To this end, fragment ab initio calculations of CASSCF/SO-RASSI/SINGLE_ANISO level were performed within MOLCAS 8.0 program package. Because **1** possesses a C_2 axis, it was sufficient to perform calculations only on two symmetry-inequivalent Dy^{III} sites of the $[Dy^{III}_4]$ cubane (Figure S4).

The calculations show that the ground-state Kramers doublet (KD) of the Dy^{III} ions is well-separated from the first excited one (Table 1). Then, the exchange interaction will only involve the ground-state KDs of each metal center. One can see that the transversal g-factors (g_x and g_y) for the ground KDs are much smaller than g_z, implying strong axiality in the ground state of Dy^{III} ions. We can therefore expect the magnetic exchange between Dy^{III} ions to be close to the Ising type.[28] The orientation of main magnetic axes of Dy centers is shown in Figure 1. Compared with previous studies on cubane systems where parallel or antiparallel alignment of spins are discussed,[29] our system shows a more involved alignment of local magnetic moments.

To model the interaction of magnetic moments on Dy sites and radicals, we take into account two circumstances. First, given the weak interaction between the radicals, observed in the density functional theory (DFT) calculations of **2**, it will be

DOI: 10.1021/acs.jpcc.8b01582
J. Phys. Chem. C 2018, 122, 11128−11135

Table 1. Energies of Eight Low-Lying KDs (cm^{-1}) at Two Inequivalent Dy^{III} Centers in 1 and the *g*-Factors in Their Ground and First Excited States

KD		Dy[a]	Dy[a]
1		0	0
2		95	109
3		150	197
4		216	272
5		264	318
6		322	396
7		466	521
8		586	636
g-tensor of the ground and first excited KDs			
1	g_x	0.00073	0.037
	g_y	0.052	0.095
	g_z	19.2	19.2
2	g_x	0.75	0.53
	g_y	1.23	0.79
	g_z	16.1	15.7

[a]Two symmetry inequivalent Dy ions.

further neglected in the exchange Hamiltonian for **1**. On the other hand, the shape of the spin-density distribution at radicals (Figure 3) shows that their interaction with both neighboring Dy ions can be considered equivalent in a good approximation. Second, given the relatively high axiality in the ground KD of Dy sites (Table 1), their exchange interaction can be well-described within the Lines approximation.[8,17] The total Hamiltonian for magnetic interaction includes both dipolar and exchange interaction within the Lines approximation (see Scheme 1)

$$\hat{H}_{tot} = \hat{H}_{dip} + \hat{H}_{exch}$$

$$\hat{H}_{exch} = -J_1(\hat{\mathbf{S}}_{Dy1}\cdot\hat{\mathbf{S}}_{Dy2} + \hat{\mathbf{S}}_{Dy1}\cdot\hat{\mathbf{S}}_{Dy3} + \hat{\mathbf{S}}_{Dy2}\cdot\hat{\mathbf{S}}_{Dy4} + \hat{\mathbf{S}}_{Dy3}\cdot\hat{\mathbf{S}}_{Dy4}) - J_2(\hat{\mathbf{S}}_{Dy1}\cdot\hat{\mathbf{S}}_{Dy4} + \hat{\mathbf{S}}_{Dy2}\cdot\hat{\mathbf{S}}_{Dy3}) - J_3(\hat{\mathbf{S}}_{Dy1}\cdot\hat{\mathbf{S}}_{R2} + \hat{\mathbf{S}}_{Dy4}\cdot\hat{\mathbf{S}}_{R2} + \hat{\mathbf{S}}_{Dy3}\cdot\hat{\mathbf{S}}_{R1} + \hat{\mathbf{S}}_{Dy2}\cdot\hat{\mathbf{S}}_{R1}) \quad (1)$$

where $\hat{\mathbf{S}}_{Dy}$ and $\hat{\mathbf{S}}_{R}$ are spin operators of Dy^{III} and radical referring to the spin $S = 5/2$ of Dy^{III} ion and $S = 1/2$ of the radical. It is further treated using the POLY_ANISO program, as described elsewhere.[18]

Scheme 1. Geometry of the Exchange Interactions in 1

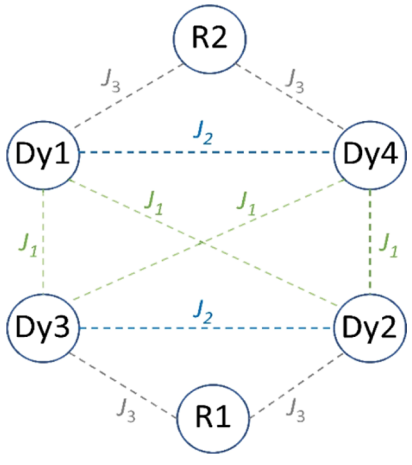

Dipolar interaction was calculated straightforwardly, using the ab initio data for Dy sites (Table 1) and considering the radical centered at the C_2 bond of the corresponding tetrazine ring (Figure 3). The three exchange parameters in eq 1 were determined by fitting the magnetic susceptibility. The best fit yields $J_1 = -0.005$, $J_2 = -0.025$, and $J_3 = -3.2$ cm^{-1} (Figure S5). Because the Dy^{III} ions are strongly axial, $g_x, g_y \ll g_z$ (Table 1), the total magnetic interaction (exchange + dipolar) attains an Ising form when projected on the ground KD of Dy sites,[8] with the parameters given in the last column of Table 2

$$\hat{H} = -\sum_{(ij)} J_{ij} s_i s_j \quad (2)$$

Table 2. Parameters of Magnetic Interactions (Dipolar and Exchange) in 1 Entering eq 2

pair	J_{dip}	J_{exch}	$J = J_{dip} + J_{exch}$
Dy1−Dy2	−2.56	−0.096	−2.66
Dy1−Dy3	−0.92	−0.11	−1.03
Dy1−Dy4	−2.85	−0.47	−3.32
Dy1−R2	−0.30	−15.26	−15.56
Dy3−Dy4	−2.17	−0.080	−2.25
Dy3−R1	−0.27	−15.24	−15.51

where s_i is either the pseudospin 1/2 of the corresponding Dy^{III} ion or the true spin 1/2 of the radical. J_{exch} parameters entering J_{ij} in eq 2 are calculated from J_i in eq 1 by rescaling the latter to the pseudospin 1/2 of dysprosium ions and multiplying them by cosine of the angle between the anisotropy axes of *ij* pairs.[30]

To understand the origin of the blocking barrier in **1**, we used an earlier developed approach to outline the relaxation path.[31] The low-energy exchange levels are separated in Ising doublets, for which the transversal *g*-factors are exactly zero by virtue of Griffith's theorem.[32] Table 3 shows that quantum tunneling of magnetization (QTM) within the ground and first excited doublets is almost suppressed (these doublets are practically degenerate). At the same time, the next excited state is a quartet (Figure 4), whose quasidegeneracy can give rise to a tunneling of magnetization. The tunneling splitting within the doublets 3 and 4 (4×10^{-6} cm^{-1}) and between them (4×10^{-5}

Table 3. Energy of the Low-Lying Exchange States of 1 and Main *g*-Factor of the Ground and First Excited Exchange Doublets

energy (cm^{-1})	*g*-factor
0	$g_z = 12.3$
0.000000	
3.483231	$g_z = 68.4$
3.483231	
7.920883	
7.920887	
7.920921	
7.920926	
8.127443	
8.127447	
8.127494	
8.127497	
...	

DOI: 10.1021/acs.jpcc.8b01582
J. Phys. Chem. C 2018, 122, 11128−11135

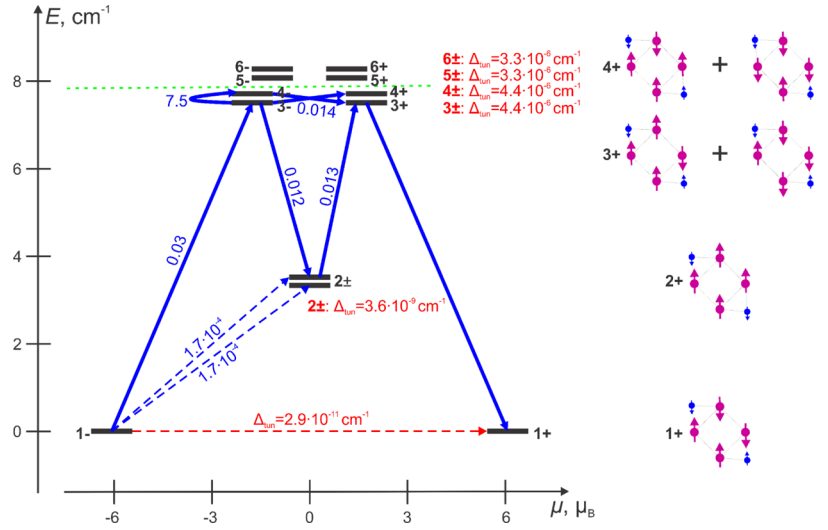

Figure 4. Low-lying exchange spectrum and magnetization blocking barrier in **1**. Each exchange level is placed according to the projection of its magnetic moment on the main magnetic axis of the ground exchange doublet. The exchange levels with the same number are the two components of the corresponding exchange doublet. The numbers accompanying the blue arrows are the average magnetic moment matrix element (in μ_B) between the corresponding components, whereas Δ_{tun} shows the intrinsic tunneling gap within the doublets. The green dashed line shows the position of the magnetization blocking barrier. The relative orientation of the local magnetic moments for one of the two components of each doublet state is shown schematically on the right side.

cm^{-1}) is significantly larger than that in the ground state (Figure 4). This is easily understood by the fact that the tunneling process requires the reversal of the two Dy momenta in the former and of all momenta in the latter case. Although the intrinsic tunneling gaps in the excited quartet are remarkably small, the induced tunneling gap via transversal internal magnetic field is 1 order of magnitude larger. Indeed, for a magnetic moment matrix element between 3± and 4∓ of 0.014 μ_B (Figure 4) in a typical internal field of several tens of mT (originating from neighbor molecules with large magnetic moments, Table 3), the Zeeman tunneling splitting between these states is expected to amount several 10^{-4} cm^{-1}. This will give the main contribution to the tunneling relaxation rate between 4−, 3− and 4+, 3+ states. Besides, the transversal Zeeman interaction will contribute to the direct relaxation process via the states 2± (Figure 4). On the other hand, the matrix elements of magnetic moment between the doublets 1, 2, 3, and 4 to the doublets 5 and 6 are negligible ($\sim 10^{-4}$ μ_B). This explains why the highest states involved in the relaxation path are ±3 and ±4, as outlined by the blue arrows in Figure 4.

Remarkably, the energy of this excited quartet, 7.9 cm^{-1} matches well with the experimentally extracted barrier 8.6 cm^{-1}. At temperatures higher than this barrier, the dominant relaxation process will correspond to magnetization reversal on individual dysprosium ions, which is expected to be fast, given the relatively large transversal g_y components of the **g**-tensor in the ground KDs of the Dy^{III} ions, ranging as 0.05−0.1 (Table 1). The fast QTM on the Dy sites is the reason for the suppression of magnetization blocking at temperatures of several kelvin (Figure S1). The ultimate reason for the observation of magnetization blocking at low temperatures in **1** is the lack of magnetic frustration in the ground state, resulting in a well-separated ground doublet (Table 3). This is similar to the situation encountered in a series of $Dy_nSc_{3-n}N@C_{80}$ compounds, where the tridysprosium complex featured worse SMM behavior than the didysprosium one because of the magnetic frustration in the ground state.[33]

On the basis of the calculated exchange states, we next investigate the equilibrium single-crystal magnetization of **1** (such magnetization curves would pass through the middle of magnetic hysteresis loops in Figure 2). To this end, for each direction of the applied field, one should sum up the $M(H)$ contributions from 18 complexes in a unit cell having different orientations in the crystal (calculated orientations in Cartesian coordinates are given in Tables S5 and S6). This means that for a reference molecule, for which the ab initio calculations have been done, one should make calculations of $M(H)$ for magnetic fields rotated from the applied one by angles corresponding to the relative orientation of molecules respective to the reference one. Note that for all molecules, we consider only the projection of their magnetic moment on the direction of the applied field. However, in the attempt to compare the calculated results with the measured magnetization, we face the problem that the direction of the applied field, with respect to the crystallographic axes, corresponding to ferromagnetic and antiferromagnetic projection (Figure 2a,b, respectively) is unknown. Therefore, we first need to find these projections from our calculations.

Given that these projections have never been extracted theoretically, we describe the methodology in more details here. The definition of ferromagnetic and antiferromagnetic projection is given in Figure 5a,b, respectively. It is only applied to noncollinear spin patterns, which is the case of our complex **1** (Figure 1). For the ferromagnetic projection, the magnetic moment changes steplike from $-M$ to M when crossing the point $H = 0$. For the antiferromagnetic projection, with the increase of magnetic field, the moment first jumps from $-M$ to 0; then, it remains at zero value in some interval of fields determined by the strength of magnetic interaction between the spins; finally, it jumps to the value M. These distinct behaviors of magnetization are clearly seen in Figure 2. It is clear, therefore, that the theoretical determination of ferromagnetic and antiferromagnetic projections should be based on the search of directions of the applied field corresponding to minimal and maximal magnetization at field

DOI: 10.1021/acs.jpcc.8b01582
J. Phys. Chem. C 2018, 122, 11128−11135

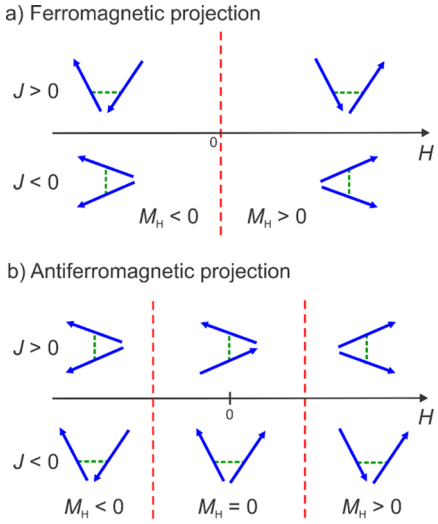

Figure 5. Ferromagnetic (a) and antiferromagnetic (b) projections of a system of two noncollinear spins. The dashed green lines denote the exchange interaction between spins (J), whereas the vertical dashed red lines are the values of the applied field (H) at which the magnetization changes by jump.

values not exceeding the limits of the field interval corresponding to low/zero magnetization in the antiferromagnetic projection (Figure 2b).

Given the complexity of the determination of the extremal values of the total momentum for 18 arbitrarily oriented complexes, we simplified the approach by considering only the ground and the first excited exchange doublets of the complexes. This limitation is justified by the large g-factor of the first excited doublet (Table 3) and relatively low value of applied field not exceeding 0.4 T (the boundary of the low-M domain in the antiferromagnetic projection, Figure 2b). With the knowledge of the main values of the g-tensor of the ground and first excited exchange doublets (Table 3) and the corresponding orientation of the main anisotropy axes (Figure 1b, Tables S5 and S6), we can calculate the magnetization by the Gibbs formula

$$M_\alpha(\mathbf{H}, T) = \sum_r \frac{\sum_{l,m} \mu_B g_z^{(l)} m \vec{e}_r^{(l)} \cdot \vec{\xi}_\alpha \, e^{-E_{rlm}/kT}}{\sum_{l,m} e^{-E_{rlm}/kT}} \quad (3)$$

where r numbers the molecules (r = 1, ..., 18), l denotes the ground and excited doublets, m is the projection of the pseudospin $\left(m = \pm\frac{1}{2}\right)$, μ_B is the Bohr magneton, $g_z^{(l)}$ is the main component of g-tensor of state l, $\vec{e}_r^{(l)}$ is the orientation of the main magnetic axis (Figure 1b, Tables S5 and S6), $\vec{\xi}$ is the orientation of the applied field, $E_{rlm} = \mu_B g_z^{(l)} m \vec{e}_r^{(l)} \cdot \vec{\xi}_\alpha H$, and H is the magnitude of the applied field. We set the temperature to 0.03 K, the magnitude of the applied field to 0.4 T, and varied the direction of the field till the maximum and minimum values of the magnetization of the unit cell. The obtained directions are the following: $\vec{\xi}_{max} = \{0.703711,\ 0.703787,\ -0.097336\}$ and $\vec{\xi}_{min} = \{-0.659561,\ 0.177849,\ 0.730308\}$ (Figure 6a). The relative angle between them is of 66° (see Figure 6). The evolution of the lowest two exchange doublets with H for each of the 18 molecules for these two directions of the applied field is shown in Figures S7 and S8. We can see that in different molecules, the crossing of the Zeeman levels occurs at different field strengths, which is the result of their differing relative orientations with respect to the applied field. Because of the larger magnetization in the excited exchange doublets of certain molecules, we expect to see a jump in their field-dependent magnetization curves. Figure 6b,c shows the calculated $M(H)$ for the directions corresponding to the calculated ferromagnetic and antiferromagnetic projections. The calculated jumps of the magnetization reveal a remarkable agreement with the steplike features of the experimentally measured magnetization loops (compare Figures 2 and 6).

4. CONCLUSIONS

In conclusion, we have investigated by means of ab initio calculations, the experimentally observed steplike features in the hysteresis loops of a radical-bridged $[Dy^{III}_4]$ complex, within a single-crystal containing 18 molecules in the unit cell. The arrangement of magnetic moments in this complex is found to be strongly noncollinear. The theoretically calculated

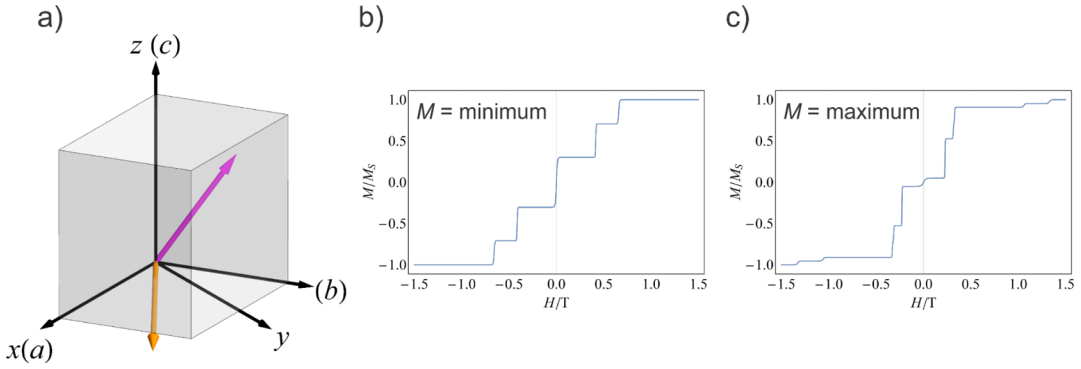

Figure 6. (a) Schematic representation of the monoclinic cell of **1**. a, b, and c are the crystallographic axes and x, y, and z are the Cartesian axes used in this work. The direction of the applied field corresponding to the maximum/minimum magnetization is shown by the orange/magenta arrow; (b) calculated total magnetization of 18 molecules from the unit cell of **1** at 0.03 K vs applied field, in the direction corresponding to the minimum of magnetization at 0.4 T; and (c) the same as (b) for the direction of the field corresponding to the maximum of magnetization at 0.4 T (see the text for details).

DOI: 10.1021/acs.jpcc.8b01582
J. Phys. Chem. C 2018, 122, 11128−11135

barrier of relaxation of magnetization is of exchange type, the height being in a remarkable agreement with the extracted one from the magnetization decay measurements. For a unit cell containing 18 arbitrarily oriented molecules, we managed to theoretically find the ferromagnetic and antiferromagnetic projections and succeeded to reproduce the basic steplike features observed in hysteresis loop measurements. Thus, combining ab initio methodologies with accurate magnetization measuring techniques, the present study affords a level of insight into the microscopic magnetic properties that is unprecedented for a spin structure of such complexity. The obtained results open the way for the investigation of the profound influence that crystal-packing effects and molecular orientation can exert on the bulk magnetic properties of molecule-based materials.

■ ASSOCIATED CONTENT

Supporting Information

The Supporting Information is available free of charge on the ACS Publications website at DOI: 10.1021/acs.jpcc.8b01582.

Magnetic hysteresis loop, magnetization decay measurements, details of ab initio calculations, calculated versus measured magnetic susceptibility and magnetization data of **1**, orientation of the main anisotropy axes of all 18 molecules of **1**, evolution of the low-lying exchange states with the applied field for all 18 molecules from the unit cell of **1**, and EPR measurements of **2** (PDF)

■ AUTHOR INFORMATION

Corresponding Author

*E-mail: liviu.chibotaru@kuleuven.be.

ORCID

Veacheslav Vieru: 0000-0001-6375-4537

Stephen Hill: 0000-0001-6742-3620

Notes

The authors declare no competing financial interest.

■ ACKNOWLEDGMENTS

We would like to thank the Murugesu Group for providing us the structure of the investigated complex and its dc magnetic data. V.V. acknowledges the postdoctoral fellowship of Fonds Wetenschappelijk Onderzoek-Vlaanderen (FWO, Flemish Science Foundation). N.I. is an overseas researcher under Postdoctoral fellowship of the Japanese Society for the Promotion of Science. W.W. thanks the EU for financial support within the FP7 FET-Proactive project MoQuaS N. 610449 and with the Agence Nationale de la Recherche project MolQuSpin, N. ANR-13-BS10. Work at the National High Magnetic Field Laboratory is supported by the US National Science Foundation (NSF grant nos. DMR-1157490 and DMR-1644779) and the State of Florida. S.H. acknowledges the support of the NSF (DMR-1610226).

■ REFERENCES

(1) Sessoli, R.; Gatteschi, D.; Caneschi, A.; Novak, M. A. Magnetic Bistability in a Metal-ion Cluster. *Nature* **1993**, *365*, 141−143.

(2) Christou, G.; Gatteschi, D.; Hendrickson, D. N.; Sessoli, R. Single-Molecule Magnets. *MRS Bull.* **2000**, *25*, 66−71.

(3) Timco, G. A.; Carretta, S.; Troiani, F.; Tuna, F.; Pritchard, R. J.; Muryn, C. A.; McInnes, E. J. L.; Ghirri, A.; Candini, A.; Santini, P.; et al. Engineering the Coupling Between Molecular Spin Qubits by Coordination Chemistry. *Nat. Nanotechnol.* **2009**, *4*, 173−178.

(4) Leuenberger, M. N.; Loss, D. Quantum Computing in Molecular Magnets. *Nature* **2001**, *410*, 789−793.

(5) Bogani, L.; Wernsdorfer, W. Molecular Spintronics Using Single-molecule Magnets. *Nat. Mater.* **2008**, *7*, 179−186.

(6) Loth, S.; von Bergmann, K.; Ternes, M.; Otte, A. F.; Lutz, C. P.; Heinrich, A. J. Controlling the State of Quantum Spins with Electric Currents. *Nat. Phys.* **2010**, *6*, 340−344.

(7) Feltham, H. L. C.; Lan, Y.; Klöwer, F.; Ungur, L.; Chibotaru, L. F.; Powell, A. K.; Brooker, S. A Non-sandwiched Macrocyclic Monolanthanide Single-molecule Magnet: The Key Role of Axiality. *Chem.—Eur. J.* **2011**, *17*, 4362−4365.

(8) Chibotaru, L. F. Theoretical Understanding of Anisotropy in Molecular Nanomagnets. In *Molecular Nanomagnets and Related Phenomena*; Gao, S., Ed.; Springer, 2015; p 185.

(9) Liu, F.; Krylov, D. S.; Spree, L.; Avdoshenko, S. M.; Samoylova, N. A.; Rosenkranz, M.; Kostanyan, A.; Greber, T.; Wolter, A. U. B.; Büchner, B.; et al. Single Molecule Magnet with an Unpaired Electron Trapped Between Two Lanthanide Ions Inside a Fullerene. *Nat. Commun.* **2017**, *8*, 16098.

(10) Liu, J.; Chen, Y.-C.; Liu, J.-L.; Vieru, V.; Ungur, L.; Jia, J.-H.; Chibotaru, L. F.; Lan, Y.; Wernsdorfer, W.; Gao, S.; et al. A Stable Pentagonal Bipyramidal Dy(III) Single-Ion Magnet with a Record Magnetization Reversal Barrier over 1000 K. *J. Am. Chem. Soc.* **2016**, *138*, 5441−5450.

(11) Demir, S.; Gonzalez, M. I.; Darago, L. E.; Evans, W. J.; Long, J. R. Giant Coercivity and High Magnetic Blocking Temperatures for N_2^{3-} Radical-bridged Dilanthanide Complexes Upon Ligand Dissociation. *Nat. Commun.* **2017**, *8*, 2144.

(12) Rinehart, J. D.; Fang, M.; Evans, W. J.; Long, J. R. A N_2^{3-} Radical-bridged Terbium Complex Exhibiting Magnetic Hysteresis at 14 K. *J. Am. Chem. Soc.* **2011**, *133*, 14236−14239.

(13) Guo, F.-S.; Day, B. M.; Chen, Y.-C.; Tong, M.-L.; Mansikkamäki, A.; Layfield, R. A. A Dysprosium Metallocene Single-Molecule Magnet Functioning at the Axial Limit. *Angew. Chem., Int. Ed.* **2017**, *56*, 11445−11449.

(14) Neese, F. The ORCA Program System. *Wiley Interdiscip. Rev.: Comput. Mol. Sci.* **2012**, *2*, 73−78.

(15) Aquilante, F.; Autschbach, J.; Carlson, R. K.; Chibotaru, L. F.; Delcey, M. G.; De Vico, L.; Galván, I. F.; Ferré, N.; Frutos, L. M.; Gagliardi, L.; et al. Molcas 8: New Capabilities for Multiconfigurational Quantum Chemical Calculations Across the Periodic Table. *J. Comput. Chem.* **2016**, *37*, 506−541.

(16) Chibotaru, L. F.; Ungur, L. Ab Initio Calculation of Anisotropic Magnetic Properties of Complexes. I. Unique Definition of Pseudospin Hamiltonians and Their Derivation. *J. Chem. Phys.* **2012**, *137*, 064112.

(17) Lines, M. E. Orbital Angular Momentum in the Theory of Paramagnetic Clusters. *J. Chem. Phys.* **1971**, *55*, 2977−2984.

(18) Chibotaru, L. F.; Ungur, L.; Aronica, C.; Elmoll, H.; Pilet, G.; Luneau, D. Structure, Magnetism, and Theoretical Study of a Mixed-valence $Co^{II}_3Co^{III}_4$ Heptanuclear Wheel: Lack of SMM Behavior Despite Negative Magnetic Anisotropy. *J. Am. Chem. Soc.* **2008**, *130*, 12445−12455.

(19) Wernsdorfer, W. From Micro- to nano-SQUIDs: Applications to Nanomagnetism. *Supercond. Sci. Technol.* **2009**, *22*, 064013.

(20) Wernsdorfer, W.; Chakov, N. E.; Christou, G. Determination of the Magnetic Anisotropy Axes of Single-molecule Magnets. *Phys. Rev. B: Condens. Matter Mater. Phys.* **2004**, *70*, 132413.

(21) Li, M.; Ako, A. M.; Lan, Y.; Wernsdorfer, W.; Buth, G.; Anson, C. E.; Powell, A. K.; Wang, Z.; Gao, S. New Heterometallic $[Mn^{III}_4Ln^{III}_4]$ Wheels Incorporating Formate Ligands. *Dalton Trans.* **2010**, *39*, 3375−3377.

(22) Abbas, G.; Lan, Y.; Kostakis, G. E.; Wernsdorfer, W.; Anson, C. E.; Powell, A. K. Series of Isostructural Planar Lanthanide Complexes $[Ln^{III}_4(\mu_3\text{-}OH)_2(mdeaH)_2(piv)_8]$ with Single Molecule Magnet Behavior for the Dy_4 Analogue. *Inorg. Chem.* **2010**, *49*, 8067−8072.

(23) Gatteschi, D.; Sessoli, R.; Villain, J. *Molecular Nanomagnets*; Oxford University Press, 2006.

(24) Aronica, C.; Pilet, G.; Chastanet, G.; Wernsdorfer, W.; Jacquot, J.-F.; Luneau, D. A Nonanuclear dysprosium(III)-copper(II) Complex

DOI: 10.1021/acs.jpcc.8b01582
J. Phys. Chem. C 2018, 122, 11128−11135

Exhibiting Single-molecule Magnet Behavior with Very Slow Zero-field Relaxation. *Angew. Chem., Int. Ed.* **2006**, *45*, 4659−4662.
(25) Lin, P.-H.; Burchell, T. J.; Ungur, L.; Chibotaru, L. F.; Wernsdorfer, W.; Murugesu, M. A Polynuclear Lanthanide Single-molecule Magnet with a Record Anisotropic Barrier. *Angew. Chem., Int. Ed.* **2009**, *48*, 9489−9492.
(26) Kahn, O. *Molecular Magnetism*; VCH Publishers, 1993; Chapter 12; p 303.
(27) Yamaguchi, K.; Takahara, Y.; Fueno, T. *Applied Quantum Chemistry*; Smith, V. H., Ed.; Reidel, 1986; p 155.
(28) Chibotaru, L. F.; Iwahara, N. Ising Exchange Interaction in Lanthanides and Actinides. *New J. Phys.* **2015**, *17*, 103028.
(29) Yang, E.-C.; Hendrickson, D. N.; Wernsdorfer, W.; Nakano, M.; Zakharov, L. N.; Sommer, R. D.; Rheingold, A. L.; Ledezma-Gairaud, M.; Christou, G. Cobalt Single-molecule Magnet. *J. Appl. Phys.* **2002**, *91*, 7382.
(30) Langley, S. K.; Wielechowski, D. P.; Vieru, V.; Chilton, N. F.; Moubaraki, B.; Abrahams, B. F.; Chibotaru, L. F.; Murray, K. S. A $\{Cr^{III}_2Dy^{III}_2\}$ Single-molecule Magnet: Enhancing the Blocking Temperature through 3d Magnetic Exchange. *Angew. Chem., Int. Ed.* **2013**, *52*, 12014−12019.
(31) Ungur, L.; Thewissen, M.; Costes, J.-P.; Wernsdorfer, W.; Chibotaru, L. F. Interplay of Strongly Anisotropic Metal Ions in Magnetic Blocking of Complexes. *Inorg. Chem.* **2013**, *52*, 6328−6337.
(32) Griffith, J. S. Spin Hamiltonian for Even-Electron Systems Having Even Multiplicity. *Phys. Rev.* **1963**, *132*, 316−319.
(33) Vieru, V.; Ungur, L.; Chibotaru, L. F. Key Role of Frustration in Suppression of Magnetization Blocking in Single-Molecule Magnets. *J. Phys. Chem. Lett.* **2013**, *4*, 3565−3569.

DOI: 10.1021/acs.jpcc.8b01582
J. Phys. Chem. C 2018, 122, 11128−11135